Available online at www.sciencedirect.com
ScienceDirect
Journal of Biotechnology 125 (2006) 416–424
Journal of BIOTECHNOLOGY
www.elsevier.com/locate/jbiotec

A novel real-time system to monitor cell aggregation and trajectories in rotating wall vessel bioreactors

Prakash Manley, Peter I. Lelkes *

Laboratory of Cellular Tissue Engineering, School of Biomedical Engineering, Science and Health Systems, Drexel University, Philadelphia, PA 19104, USA

Received 28 November 2005; accepted 19 March 2006

Abstract

Rotating wall vessel bioreactors (RWVs) constitute dynamic suspension culture venues for tissue engineering. Quantitative real-time assessment of the kinetics of cell–cell aggregation in RWVs can yield mechanistic information about the initial steps leading to the assembly of individual cells into tissue-like constructs. In our imaging system, fluorescently labeled cells suspended in a HARV-type RWV were irradiated by a laser-beam. Emission was recorded by a camera mounted at 90° to the excitation plane. Using macro lenses, the system identified ~5 μm particles from a 5 cm working distance, distinguished aggregated 20 μm microspheres from larger (45 and 90 μm) microspheres, and plotted local trajectories of microspheres and cells. Sizes of PC12 cells assessed by our system matched conventional measurements. We validated the system's ability to follow HepG2 and PC12 aggregation in real time over 24 h of RWV culture. Taken together, our system provides the means to measure and analyze in real time the processes that lead to the 3D tissue-like assembly of diverse cell types into spheroids. Future studies include development of intelligent feedback algorithms, allowing automatic control over RWV rotational speed required to maintain aggregating cells and nascent tissue in continual free fall.

Keywords: RWV bioreactor; PC12 cells; HepG2 cells; Real-time monitoring; CCD; Micro-gravity; aggregation

1. Introduction

The RWV bioreactor is a widely acknowledged venue for three dimensional tissue engineering and simulated microgravity on earth (Goodwin et al., 1993; Unsworth and Lelkes, 1998). It has been proved to facilitate aggregation and been used to support chondrogenesis for bone repair and replacement (Duke et al., 1993), and to assist in the aggregation of embryonic limb cells (Duke et al., 1996). The RWV provides solid

Abbreviations: RWV, rotating wall vessel bioreactor; HARV, high aspect ratio vessel; CFSE, carboxyfluorescein succinimidyl ester; CCD, charge coupled device; NTSC, National Television System Committee; FOV, field of view

* Corresponding author at: Laboratory of Cellular Tissue Engineering, School of Biomedical Engineering, Science and Health Systems, Drexel University, New College Building, Room 10302, 245 N. 15th Street, Philadelphia, PA 19104, USA.
Tel.: +1 215 762 2071 (Off)/7234 (Lab); fax: +1 215 895 4983.
E-mail address: pilelkes@drexel.edu (P.I. Lelkes).

0168-1656/$ – see front matter © 2006 Elsevier B.V. All rights reserved.
doi:10.1016/j.jbiotec.2006.03.030

body rotation of the enclosed fluid medium (Schwarz et al., 1992), and particles are continually suspended because the gravity-induced sedimentation is balanced by the upward forces produced by rotating the vessel (Nickerson et al., 2004).

Cells aggregating in bioreactors over time experience increasing mass, resulting in enhanced gravitational pull which in turn leads to increased shear stress and viscous drag acting on the aggregates. Thus for increasing aggregate sizes the rotation speed of the vessel has to be adjusted to meet solid body rotation requirements. Currently, aggregates are kept in continual free fall by empirically/manually making minor increments to the rotational speed at regular time intervals, based on experience and visual examination of the way in which the samples "tumble" in the rotating bioreactors (Duke et al., 1996). An imaging system that could detect particle motion in real time would be useful for both understanding processes leading to cell–cell aggregation as well as for designing a feedback loop that automatically can adjust the rotational speed of the RWV bioreactor based on the real-time analysis of images of particle movement captured by time lapse photography.

To date, no real-time systems exist for 3D cell aggregation measurement because of optical limitations. Experimental models of aggregation have been developed for cells seeded on micro-carrier beads in RWVs (Muhitch et al., 2000) as well as other cell systems. Traditionally the kinetics of cell aggregation are modeled based on Smoluchowski's (1917) population-balance equations (Nguyen and O'Rear, 1990). There is however, limited experimental verification for these models (Enmon et al., 2002) and no real-time system that provides instantaneous information of cell aggregate size. Gao et al. (1997) studied the motion of microcarrier particles in HARV type RWV bioreactors numerically, but their work does not include experimental verification in real-time but is based on analysis of samples extracted from the bioreactor.

In order to study cell aggregation in HARVs we focus on two different cell types, PC12 rat pheochromocytoma cells and HepG2 human hepatocellular carcinoma cells. PC12, and to a greater extent HepG2 cells, form large aggregates with histotypic epithelioid morphology in RWV culture (Lelkes et al., 2004; Khaoustov et al., 2001), unlike other cells, such as the insect ovary cell line SF-9 (Cowger et al., 1999) for example, which do not aggregate in RWV conditions.

In this study, we describe a newly designed imaging system which we used to record and analyze the motion and aggregation of PC12 and HepG2 cells in real time. Using a similar optical system with significantly lesser resolution, Pollack et al. (2000) measured trajectories of large (1 mm diameter) microcarrier particles. Qiu et al. (1999) used the same system to evaluate different kinds of microcarrier beads and selected the most suitable ones for use in RWV based cell culture. Significantly, in this study we now further advance the system developed by Pollack et al., into a true high-resolution (<2.5 μm/pixel) cell imaging device.

2. Materials and methods

2.1. Imaging components and optics

A tunable argon ion laser (BeamLok® 2060-7S Argon Ion laser, Spectra-Physics®, Irvine, CA) with adjustable output power was used for excitation of the samples in the visible wavelength range. The laser beam was directed to the sample camber (HARV, see schematic in Fig. 1) via high reflectance precision mirrors with limited losses.

A 1/2 in. charge coupled device (CCD) color video camera (Hitachi KP-D50) with a resolution of 768 (H) × 494 (V) effective pixels for NTSC systems was used for detection of fluorescence emission from the sample. A Micro-Nikkor 55 mm *f*/2.8 macro lens (Nikon) served as the primary collection lens. The use of a bellows unit (kindly loaned by Mr. Steve Miller, IMiller Optical, Philadelphia, PA) increased magnification to 4× (primary optical magnification) and ∼120× (including secondary electronic magnification).

For the initial system validation and calibration, we used Fluoresbrite® Yellow Green (YG) fluorescent polystyrene latex microspheres (20, 45 and 90 μm diameter, Polysciences Inc., Warrington, PA). When excited by the 457 nm (blue) line of the argon laser, these beads emitted a strong fluorescence signal the maximum of which was centered at 486 nm.

Two different optical filter sets were custom made for these experiments by Omega® Optical, Rego Park, NY. For the microspheres we used a band pass fil-

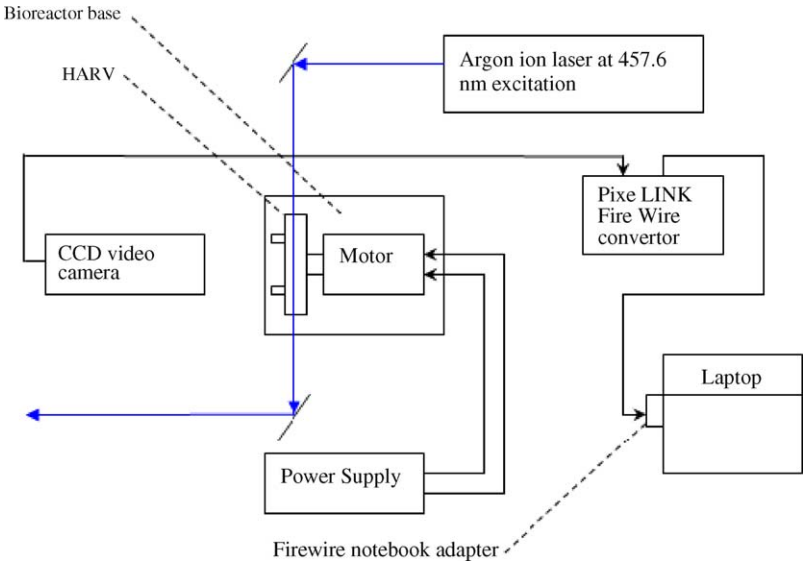

Fig. 1. Experimental setup—schematic showing individual components of the system.

ter centered at 486 nm, with 85% transmission efficiency and a full width half-maximum of 20 nm. For the CFSE stained cells, we used a 517 nm cut-on filter with approximately 87% transmission efficiency at 517 nm and very high attenuation levels below 500 nm (the excitation laser line for this case was 488 nm). Both the filters were 52 mm wide, to fit the diameter of the objective lens.

2.2. Electronic equipment

The Hitachi KP-D50 camera described earlier was connected via an IEEE 1394 Firewire 400 6 pin to 6 pin cable coaxial cable to a PixeLINK™ PL-A544 analog camera signal converter to FireWire standard, which in turn was connected to a notebook computer (DELL™ Inspiron 1100 Notebook computer with an Intel® Celeron® CPU 2.40 GHz processor) fitted with a PCI cardbus compatible FireWire Notebook Adapter (Belkin®, Compton, CA).

2.3. Image processing and analysis components

VirtualDub (http://www.virtualdub.org/), a video capture/processing utility for 32-bit Windows platforms, was used to acquire and process video clips acquired by the camera. NIH ImageJ (http://rsb.info.nih.gov/ij/) and ImagePro Plus® 5.0 (Media Cybernetics, Silver Springs, MD) were used to process the acquired video files and images, and plot size distributions.

2.4. RWV setup

For the experiments described here, the sample chamber (50 mL disposable HARV, Synthecon™ Inc., Houston TX) was mounted on a homemade rotator base constructed at the Drexel University machine shop. A 27 V dc gear motor (126A190 from Motor Technology Inc., Dayton, OH) fitted with a threaded adapter for the bioreactor, powered by a 0–30 V dc/0–3 A regulated power supply dc power supply (CSI3003X from Circuit Specialists, Inc., Mesa, AZ) was used to adjust the speed of the bioreactor rotation.

2.5. Cell culture

PC12 rat adrenal pheochromocytoma cells were used for the initial validation aggregation experiments. The cells were routinely cultured in Dulbecco's modified Eagle's medium (DMEM) supplemented with L-glutamine, containing 4.5 g/L glucose, 7.5% fetal bovine serum and 7.5% horse serum at 37 °C in a 5% CO_2 incubator, as previously described.

Since HepG2 (ATCC, HB-8065) human hepatocellular carcinoma cells rapidly form sizeable aggregates, they were used for detailed studies of aggregation kinetics. The cells were routinely cultured in minimum essential medium (MEM) with 10% FBS and 1% penicillin–streptomycin (antibiotic).

All real-time aggregation experiments were performed in colorless medium without phenol red, supplemented with 110 mg/L sodium pyruvate with pyridoxine hydrochloride, L-glutamine, 1% penicillin–streptomycin and (a) 7.5% fetal bovine serum +7.5% horse serum for PC12 cells or (b) 10% FBS for HepG2. Imaging for up to 3 h was performed outside the cell culture incubator. For the later time-point (24 h), the RWV system was returned to and run in a 37 °C, 5% CO_2 incubator until the time of measurement which again was performed outside the incubator.

2.6. Fluorophores

For intracellular fluorescent labeling we used carboxyfluorescein succinimidyl ester (CellTrace™ CFSE Cell proliferation kit, C34554 from Invitrogen, Carlsbad, CA). At recommended fluorophore concentrations (0.5–25 μM), the excitation spectrum of this probe peaks at 492 nm with an emission maximum at 517 nm. At these concentrations however, low fluorescence intensity coupled with rapid photobleaching thwarts the usefulness of the dye for our purposes. Therefore, in our experiments we loaded the cells with 5 mM CFSE. At this concentration the optical properties of the dye are altered presumably due to the formation of dimers and higher aggregates (Lelkes and Miller, 1980) resulting in a more photostable and visibly enhanced emission at 517 nm. In preliminary experiments we established that at this concentration CFSE was neither cytotoxic nor did it impair the normal aggregation process (data not shown).

2.7. Cell staining and inoculation of the RWV

For intracellular staining, the cell suspensions were pelleted (400 g for 5 min), re-suspended ($\sim 1 \times 10^6$ cells/mL) in pre-warmed PBS containing the 5 mM CFSE, and incubated for 15 min at 37 °C. The dye-loaded cells were re-pelleted by centrifugation, re-suspended in fresh pre-warmed cell culture medium and then incubated for another 30 min to ensure complete conversion of the probe. Following another round of washing (to remove unincorporated dye) the pellet was re-suspended and adjusted to the desired seeding density. Finally the cell suspension was filtered through a 20 μm cell sieve (Fisher Scientific, Pittsburgh, PA) to ensure inoculation of the cell culture vessels with a single cell suspension. For inoculation and operation of the RWV bioreactors we followed previously described techniques (Lelkes et al., 2004).

2.8. Statistical analysis

Particle size distributions were plotted by analyzing composite images containing several aggregates in focus on ImagePro Plus® 5.0. Where applicable, values listed are means ± standard deviation. Differences between samples were tested for statistical significance. Values with $p < 0.05$ were regarded as statistically significant.

3. Results

3.1. Calibration and validation of the system with fluorescent microspheres

The working distance between the camera and bioreactor face was fixed at 5.5 cm. For capturing images of individual microspheres moving within the HARV, the shutter speed was set at 1 ms. Under these conditions, the field of view (FOV) captured by the imaging apparatus was 1.5 mm × 1.125 mm. Since the images and videos were displayed with a resolution of 640 × 480 pixels on our computer monitor, the highest magnification attainable using the existing camera and optical system provided a resolution of 2.34 μm/pixel. This resolution worked well for the microspheres larger than 20 μm and also for PC12 and HepG2 cells that are ≥8 μm in diameter.

Initially the system was calibrated with 20, 45 and 90 μm fluorescent microspheres Actual images captured by the system are shown in Fig. 2, demonstrating good edge detection, and the ability to distinguish between microspheres of different sizes. In terms of accuracy of the size determinations, the dynamically measured size of samples containing only 20 μm particles ranged from 16.4 to 23.7 μm. This value is in

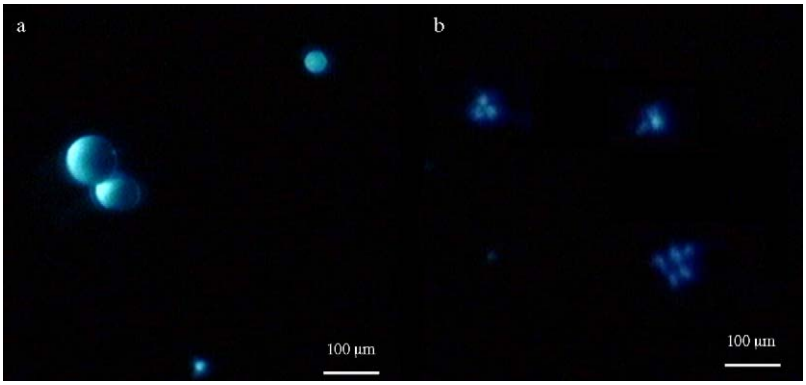

Fig. 2. Size differentiation and edge detection: (a) 20 and 45 μm fluorescent particles (Polysciences Inc.) with doublet of 90 μm particles and (b) three particle aggregate of 20 μm microspheres and two other small microsphere clusters.

reasonably good agreement with the supplier's specifications (20 μm ± 3.2 μm) for these microspheres (see also comparisons in Table 1). Importantly, the system was able to distinguish between individual larger spheres and similar sized aggregates containing several smaller spheres (Fig. 2b).

3.2. Trajectory plot

Due to the higher magnification attained here, particle or cell/aggregate trajectories can be plotted within a much smaller FOV (1.5 mm × 1.125 mm) than with existing analogous systems (Pollack et al., 2000; Qiu et al., 1999). If required, the FOV can be increased to a maximum of 12 mm × 9 mm by varying the focal length setting on the bellows unit. The trajectory followed by a 45 μm microsphere near the center of the RWV shows an almost circular path over one rotation. The image shown in Fig. 3a is a composition of several frames extracted from video recordings of the motion of a single 45 μm calibration bead. Fig. 3b and c are composite images of PC12 cell aggregates in solid body rotation, captured in real time. The red arrows illustrate the constant re-alignment of the aggregate axis with respect to the gravity vector, thus visually confirming for the first time a basic tenet of the "modeled microgravity component" of the RWV environment, i.e., the time averaged randomization of position of the rotating particles with respect to the gravitational vector.

3.3. Size distributions

To validate the system with real cells, we analyzed the size distribution of freshly dispersed individual PC12 cells. Fig. 4 shows a histogram of the dynamically measured diameters of single PC12 cells seeded in a HARV after sieving through a 20 μm cell strainer. Video recording began within the first few minutes after seeding meaning that not much aggregation had taken place yet. The mean diameter (11.8 ± 3.8 μm), as calculated from this histogram, closely matches (Table 1) PC12 diameter values reported in literature (between 6 and 14 μm, Fujita et al., 1989). The dynamically determined cell diameters also matched the diameters measured directly, of PC12s in static culture on a microscope slide, where they were distributed with a mean diameter of 10.2 μm and S.D. of ±1.7 μm ($n = 166$).

Table 1
Diameter comparisons

	Diameter values specified in data sheet or literature (mean ± S.D.) (μm)	As measured by the real-time system (μm)	Measured in static conditions under microscope
Microspheres	20 ± 3.2	18.8 ± 1.93	–
PC12	10 ± 4	11.5 ± 3.75	10.2 ± 1.72
HepG2	–	16.14 ± 5.71	15.61 ± 2.71

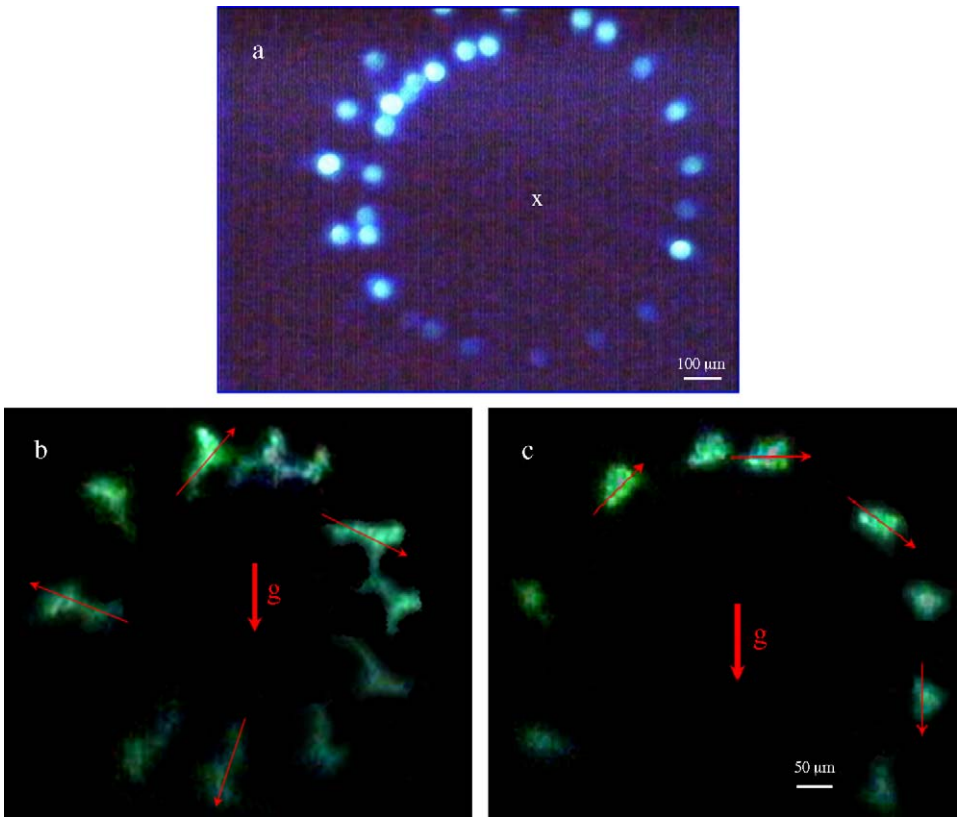

Fig. 3. Trajectory plots. (a) This was formed by composing several frames from the video. The trajectory is that of a 42 μm fluorescent particle over one rotation around the bioreactor center at 13.5 rpm. X marks the center of the bioreactor. (b and c) Two non-spherical aggregates following circular paths illustrate solid-body rotation not evident in spherical aggregates. Arrows show consistent re-alignment of the aggregate axis with respect to the gravity vector g.

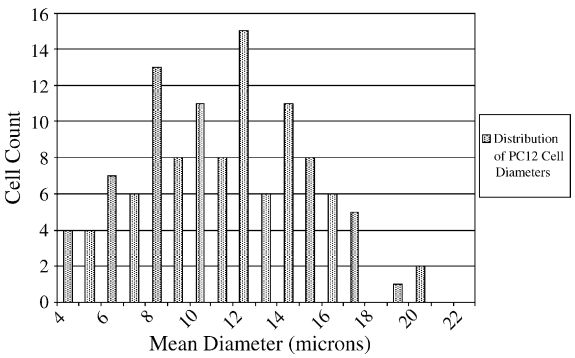

Fig. 4. Size distribution of PC12 cells. Based on ImagePro analysis of a re-suspended suspension of PC12 cells seeded in a bioreactor, consisting mostly of singlets with very few doublets of cells. Images for analysis were extracted from videos of the bioreactor rotating at 12 rpm. The data ($n = 115$) shows a mean of 11.5 μm with a standard deviation of 3.75 μm.

3.4. Cell aggregation over time

In line with previous reports in the literature of the rapid aggregation of HepG2 cells in RWV culture, we established in preliminary studies a suitable concentration (250,000 cells/mL) that would yield aggregates of controlled and reproducible size within 24 h. For assessing the aggregation kinetics, freshly re-suspended HepG2 cells were sieved through a 40 μm cell strainer and seeded as single cells at 250,000 cells/mL in the HARV. Images were captured immediately after seeding ($t = 0$), and at 1, 2, 3 and 24 h post-seeding. For comparison, we also manually evaluated under the microscope, the size distributions of the same cell populations harvested at each time point. As seen in Fig. 5a and b, at seeding, the vast majority of the cells were either seen as single cells or smaller

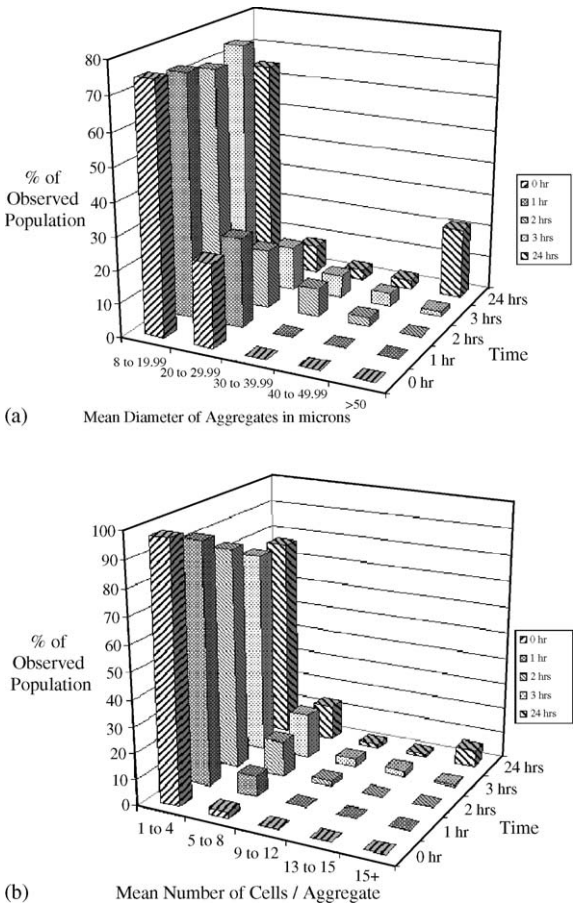

Fig. 5. HepG2 aggregation over time. (a) Percentage (of the total population analyzed) of HepG2 aggregates in each size range as viewed on the real-time imaging system over time. (b) Control experiment. Similar experimental setup, but using one RWV seeded with cells for every time point on the graph. Imaged under a phase contrast microscope.

aggregates containing up to four cells. Very few cells were initially found in the form of larger aggregates (>15 cells). This observation was true, albeit with some differences, for both the real-time and the manual measurement. Over time, the number of single cells/smaller aggregates decreased with a concomitant increase in the number of larger aggregates. Of note, both the real-time and the manual measurements are capable of picking up the transient increase in the number of mid-sized aggregates. Similar results (not shown) were also obtained measuring in real-time the aggregation of PC12 cells. Taken together, these experiments establish the high-resolution of our system which can accurately measure cell size distributions as well as aggregation kinetics in real time.

4. Discussion

We have developed for the first time, an enabling technology that supports visual examination and analysis of the aggregation processes of live cells in RWV culture. This system provides an efficient countermeasure to the tedious manual measurement pursued traditionally, on multiple samples under the microscope. The optical principle of our system is not unlike other detection methodologies like flow-cytometry differing only by virtue of the type of output. While flow cytometers use PMT detectors and deliver voltage output pulses proportional to the intensity of fluorescence, our prototype uses a CCD video camera which allows real-time visual examination of the sample chamber by providing an electronic image. The limitations of this system in its existing configuration are related to the specifics of optic and electronic equipment used. The current resolution is sufficient to capture individual small cells the size of PC12s. Capturing images of smaller cells such as PBMCs would require cameras with higher resolution. On the other hand, such high-resolution cameras would also allow for increasing FOV while maintaining a resolution of 2–3 μm/pixel. Another limitation of the current system is the restriction to FOVs closer to the center of the HARV because of the relatively slow image acquisition speed of 14 frames per second. Particles rotating at faster speeds near the edge of the HARV appear as streaks (data not shown). This impediment could be overcome using higher acquisition rates of 60 frames per second. Currently, efforts are under way to construct such an improved system.

Photo-bleaching of the fluorophore is a concern. Periodic excitation for short durations of approximately 3 min at a time did not cause much photobleaching of CFSE at 5 mM. However, when irradiated continuously for approximately 10 min, a small volume of cells in a 1.5 mm^3 volume of the FOV in the center of the HARV were found to be photo-bleached. This is because this small section is continuously irradiated by the laser beam while the regions away from the center are irradiated only momentarily, two times every rota-

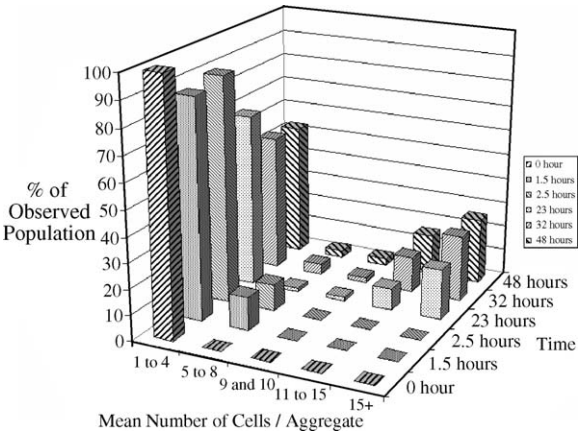

Fig. 6. PC12 aggregation over time (control, cells stained with 5 mM CFSE and counted manually). Experimental setup included one RWV (placed in an incubator) seeded with cells for each time point on the graph. Imaging was performed under a phase contrast microscope. Presence of larger aggregates (11 cells and more) at 48 h indicates that aggregation has not been impeded.

tion. Lower laser power such as those provided by laser diodes would be sufficient as an excitation source for this application. However, very low excitation power might require a more sensitive, low light level camera.

The use of high concentrations of CFSE as a fluorophore has solved numerous problems encountered during our preliminary feasibility studies. The fluorescent microspheres used for the calibration studies were characterized by uniform fluorescence of high intensity (Figs. 2 and 3). None of the more conventional fluorophores tested at recommended concentrations such as DiI, or 585 nm quantum dots proved sufficient either in terms of intensity, photostability or uniformity of cell labeling. Similarly, CFSE at regular concentrations of 5 μM was inadequate in terms of intensity. By contrast, cells labeled with high concentrations (5 mM) of CFSE fulfilled the required criteria. Under our conditions, the cells appeared uniformly stained and the fluorescence intensity was sufficient to image the cells for up to 24 h. Importantly, in preliminary studies, we ascertained that this high concentration of CFSE did not impair cell function or affect cell aggregation (Fig. 6). Thus the rate of proliferation of CFSE loaded PC12 cells and their neuritogenic response to NGF was indistinguishable from those of untreated controls (manuscript in preparation).

In analyzing the fluorescent images captured either in real time or manually under the microscope, we noted similarities but also some differences in results obtained from the two techniques. Both systems noted the decrease in the number of smaller aggregates over time concomitant with an increase in the percentage of larger (>40 μm) aggregates in suspension (Fig. 5a and b) over time. The larger number of singlets and smaller number of larger aggregates in the control sample is presumably due to the disruption of the aggregates in the wake of their extraction from the sample chamber. In particular we note that we observed numerous very large aggregates between 150 and 200 μm wide in the real-time system, which were not observed after manual manipulations of the sample in the control, which probably broke up the larger aggregates. Moreover, the transient kinetics of appearance and disappearance of aggregates of intermediate size, as observed in the real-time system but not in the manually manipulated controls is in line with the predictions of theoretical models (manuscript in preparation).

In this study we have developed a novel real-time imaging system for cell suspensions rotating in RWV bioreactors. In our current configuration, this device is comparable to but is a distinct advancement over previously described systems (Pollack et al., 2000), in that we are able to monitor, record and analyze in real-time, the motion and aggregation of individual cells. The advantages of this high-resolution system are many, for example, under optimized conditions, using our high-resolution, we should be able to detect and describe specific mechanisms of cell aggregation leading to formation of tissue-like assemblies such as formation of inter-cellular bridges (Vidulescu et al., 2004). Similarly, using multi-color fluorescence of differentially labeled cells, we predict that we can follow aggregation kinetics and mechanisms of heterotypic cell cultures. Finally, in practical terms, our system could represent the beginning of a complex feedback regulatory system in which complex algorithms based on image/pattern recognition could be employed to adapt the rotational speed of the RWV system in accordance with the increasing aggregate size. This latter approach would constitute an elegant and necessary countermeasure to the hitherto empirical attempt to maintain solid body rotation in a population of cell aggregates with increasing sizes.

Acknowledgements

Equipment for this project was funded, in part, by NASA grant NAG 97-HEDS-02. We thank Mr. Mark R. Contarino and Dr. Som Tyagi for invaluable discussions while selecting optics for the system. We gratefully acknowledge Mr. Steve Miller's patience and untiring help acquiring the optics and software required. PM would also like to thank Mr. Eric M. Troop for his help with RWV culture, and the members of the Cellular Tissue Engineering Lab at Drexel University.

References

Cowger, N.L., O'Connor, K.C., Hammond, T.G., Lacks, D.J., Navar, G.L., 1999. Characterization of bimodal cell death of insect cells in a rotating-wall vessel and shaker flask. Biotechnol. Bioeng. 64 (1), 14–26.

Duke, P.J., Daane, E.L., Montufar-Solis, D., 1993. Studies of chondrogenesis in rotating systems. J. Cell. Biochem. 51 (3), 274–282 (review).

Duke, P.J., Daane, E.L., Arizpe, J., Montufar-Solis, D., 1996. Chondrogenesis in aggregates of embryonic limb cells grown in a rotating wall vessel. Adv. Space Res. 17 (6/7), 289–293.

Enmon Jr., R.M., O'Connor, K.C., Song, H., Lacks, D.J., Schwartz, D.K., 2002. Aggregation kinetics of well and poorly differentiated human prostate cancer cells. Biotechnol. Bioeng. 80 (5), 580–588.

Fujita, K., Lazarovici, P., Guroff, G., 1989. Regulation of the differentiation of PC12 pheochromocytoma cells. Environ. Health Perspect. 80, 127–142 (review).

Gao, H., Ayyaswamy, P.S., Ducheyne, P., 1997. Dynamics of a microcarrier particle in the simulated microgravity environment of a rotating-wall vessel. Microgravity Sci. Technol. 10 (3), 154–165.

Goodwin, T.J., Schroeder, W.F., Wolf, D.A., Moyer, M.P., 1993. Rotating-wall vessel co-culture of small intestine as a prelude to tissue modeling: aspects of simulated microgravity. Proc. Soc. Exp. Biol. Med. 202 (2), 181–192.

Khaoustov, V.I., Risin, D., Pellis, N.R., Yoffe, B., 2001. Microarray analysis of genes differentially expressed in HepG2 cells cultured in simulated microgravity: preliminary report. In Vitro Cell Dev. Biol. Anim. 37 (2), 84–88.

Lelkes, P.I., Miller, I.R., 1980. Perturbations of membrane structure by optical probes. I. Location and structural sensitivity of merocyanine 540 bound to phospholipid membranes. J. Membr. Biol. 52 (1), 1–15.

Lelkes, P.I., Unsworth, B.R., Saporta, S., Cameron, D.F., Gallo, G., 2004. Culture of neuroendocrine and neuronal cells for tissue engineering. In: Vunjak-Novakovic, G., Freshney, R.I. (Eds.), Culture of Cells for Tissue Engineering. Wiley-Liss Inc., New York, NY.

Muhitch, J.W., O'Connor, K.C., Blake, D.A., Lacks, D.J., Rosenzweig, N., Spaulding, G.F., 2000. Characterization of aggregation and protein expression of bovine corneal endothelial cells as microcarrier cultures in a rotating-wall vessel. Cytotechnology 32, 253–263.

Nguyen, P.D., O'Rear, E.A., 1990. Temporal aggregate size distributions from simulation of platelet aggregation and disaggregation. Ann. Biomed. Eng. 18 (4), 427–444.

Nickerson, C.A., Ott, M.C., Wilson, J.W., Ramamurthy, R., Pierson, D.L., 2004. Microbial responses to microgravity and other low-shear environments. Microbiol. Mol. Biol. Rev. 68 (2), 345–361 (review).

Pollack, S.R., Meaney, D.F., Levine, E.M., Litt, M., Johnston, E.D., 2000. Numerical model and experimental validation of microcarrier motion in a rotating bioreactor. Tiss. Eng. 6 (5), 519–530.

Qiu, Q.Q., Ducheyne, P., Ayyaswamy, P.S., 1999. Fabrication, characterization and evaluation of bioceramic hollow microspheres used as microcarriers for 3D bone tissue formation in rotating bioreactors. Biomaterials 20 (11), 989–1001.

Schwarz, R.P., Goodwin, T.J., Wolf, D.A., 1992. Cell culture for three-dimensional modeling in rotating-wall vessels: an application of simulated microgravity. J. Tiss. Cult. Meth. 14, 51–58.

Smoluchowski, M.V., 1917. Versuch einer mathematischen theorie der koagulationskinetik kolloider loesungen. Z. Phys. Chem. 92, 129–168.

Unsworth, B.R., Lelkes, P.I., 1998. Growing tissues in microgravity. Nat. Med. 4 (8), 901–907.

Vidulescu, C., Clejan, S., O'Connor, K.C., 2004. Vesicle traffic through intercellular bridges in DU 145 human prostate cancer cells. J. Cell. Mol. Med. 8 (3), 388–396.